

Hydro-mechanical modelling of geological CO₂ storage and the study of possible caprock fracture mechanisms

N. Guy,¹⁻² D.M. Seyedi,¹ F. Hild²

BRGM, Natural Risks & CO₂ Storage Safety Division, 3 av. Claude Guillemin, BP 36009, F-45060 Orléans Cedex 2, France

LMT-Cachan, ENS de Cachan/CNRS/UPMC/PRES UniverSud Paris, 61 av. du Président Wilson, F-94235 Cachan Cedex, France

Corresponding author: D.M. Seyedi, e-mail: d.seyedi@brgm.fr, tel: +33238643408

The present study discusses the results of a large scale finite element modelling of a hypothetical underground carbon dioxide (CO₂) storage operation. The hydro-mechanical properties of the materials modelled are chosen to be representative of a potential injection site. For high injection rates, local effective stress modifications may lead to various fracture mechanisms induced by shear or tensile stresses depending on the initial conditions. The results show the influence of the initial stress state on the possible fracture mechanisms. Sustainable injection rate maps are introduced that provide a first order estimate depending on initial stress states. The case of rock fracturing due to tensile stresses is treated. The stress intensity factor is used as the driving parameter describing the growth of initial vertical cracks. A probabilistic model based on rock heterogeneity is used to evaluate the probability of the formation and propagation of crack networks. The results show that a crack network can be generated. This crack network saturates quickly after the first crack activations.

Keywords: CO₂ geological storage; storage integrity; sustainable injection rate; hydromechanical modeling; Rock fracture, Probabilistic method

Introduction

Underground storage of CO₂ in deep geological formations is considered as being a potential solution for reducing the emission of greenhouse gases into the atmosphere (IPCC 2005). The integrity of caprock is a key issue to characterize storage performance and safety because caprock is assumed to prevent CO₂ leakage from the injection zone up to the upper layers and earth surface.

Recent studies have shown that gas injection into deep permeable formations induce changes of the total and effective stresses in the reservoir and its surrounding layers through pore pressure increase (e.g., Rutqvist *et al.* 2008, Vidal-Gilbert *et al.* 2009, Rohmer and Seyedi 2009). This local stress modification may lead to damage for high pressure build-ups. Mechanically induced degradation is split into two cases, namely, rock fracturing induced by tensile stresses

and fault slip activation, or reactivation, or rock plasticity induced by shear stresses (e.g., Rozhko *et al.* 2007, Rutqvist *et al.* 2008, Soltanzadeh and Hawkes 2009, Rohmer and Seyedi 2009). The prevalent degradation mechanism to study depends on the injection process, and on site and rock properties.

Rutqvist *et al.* (2008) showed through a coupled reservoir geomechanical simulation of CO₂ injection into a multilayered site using a two-dimensional plane-strain model that the maximum sustainable overpressure is strongly dependent on the *in situ* stress state. In an extensional stress regime ($\sigma_h = 0.7\sigma_v$), reactivation of steeply dipping fractures is most likely to occur, whereas in a compressional stress regime ($\sigma_h = 1.5\sigma_v$), reactivation of shallowly dipping fractures is most likely at a higher injection pressure (Rutqvist *et al.*, 2008).

Soltanzadeh and Hawkes (2009) investigated the stress change within and surrounding reservoirs during fluid injection or production using Eshelby's theory of inclusions for a poroelastic material. Coulomb's failure criterion is then considered for the prediction of fault reactivation. Their results demonstrate that, during fluid injection into a reservoir in an extensional stress regime (*i.e.*, $|\sigma'_h| < |\sigma'_v|$), only faults located in rocks overlying and underlying the reservoir may reactivate. For a compressional stress regime (*i.e.*, $|\sigma'_h| > |\sigma'_v|$), fault reactivation is likely to occur within the reservoir and in the vicinity of its boundary.

The aim of this study is to present a combined analysis of both shear and tensile failure for a representative reservoir geometry and for various initial stress regimes. The results are presented as sustainable injection rate maps. Such type of maps, built for each specific site, can be used to estimate the suitable injection rate as a function of mechanical characteristics of the site. A probabilistic framework is finally presented to take into account the effect of mechanical heterogeneities on the fracturing probability of the caprock for high injection rates.

Hydro-mechanical modeling

The following numerical simulations of CO₂ injection represent a simplified but realistic case to define different failure mechanisms that may be generated in reservoirs. The numerical analyses are performed using the hydromechanical routines of Code_Aster (EDF R&D, 2008), which is a general purpose thermo-mechanical finite element code developed by EDF. A large cylinder of ground that has a diameter of 30 km and a height of 2.8 km is considered. It is made of several geological layers as shown in Figure 1. A plane that has a height equal to the ground cylinder height and a length equal to the ground cylinder radius is meshed. The three-dimensional aspects are taken into account through axisymmetric simulations. An isotropic and elastic behaviour is assumed for each geological layer. The injection procedure is described by a gradual increase of the injection along the tubing, which has a length of 25 m. The tubing centre is located in the middle height of the reservoir, at a depth of 1,400 m. The reservoir is 50 m thick and sealed by a 100 m thick caprock that has low permeability and porosity. In a CO₂ injection process, CO₂ is always stored at supercritical conditions. Supercritical CO₂ has a low viscosity and a high density even if the latter is less than the density of water. In the present case, fluids are represented by water for the sake of simplicity. However, an equivalent injection rate r_e is introduced to characterize the relevant loading conditions. The equivalent injection rate is considered in terms of volume by assuming that the stored CO₂ in the geological formation has a mass density of the order of 780 kg/m³ (Bachu 2003). The use of this equivalent rate enables us to obtain acceptable results in terms of pressure build-up in the reservoir by resorting to monophasic simulations (see Appendix A). The lateral boundaries are far enough from the injection well to reproduce “infinite” boundary conditions. The injection rate increase is slow enough to reach a stable stress state for every time step of the simulations. It is considered that the stress state observed in the

geological formation is associated with a corresponding injection rate. An injection rate description of the loading is preferred to a pressure description. When an injection pressure is prescribed, the results depend on the considered injection length and well geometry. An injection rate description enables the results to become less dependent on these details at a given distance from the well.

The domain is considered as a saturated porous medium (Biot 1941). The conservation equations read

$$\operatorname{div}(\underline{\sigma}) + r \underline{g} = 0 \quad (1)$$

and

$$\dot{r}_m + \operatorname{div}(\underline{M}) = 0 \quad (2)$$

where $\underline{\sigma} = \underline{\sigma}' + \sigma_p \underline{I}$ is the total stress tensor, $\sigma_p = -bp$, with b Biot's coefficient, p the pore pressure, \underline{g} gravity vector and \underline{M} the mass flux. Furthermore, $r = r_m + r_0$ is the average global mass, r_0 the initial average global mass and r_m the incoming mass. The porosity change is expressed as

$$d\phi = (b - \phi)d\varepsilon_v \quad (3)$$

where $\varepsilon_v = \operatorname{trace}(\underline{\varepsilon})$, with $\underline{\varepsilon}$ the strain tensor. The incoming mass change reads

$$\rho_l \phi(1 + \varepsilon_v) = \rho_l^0 \phi^0 + r_m \quad (4)$$

where ρ_l denotes the fluid density, ρ_l^0 the initial fluid density, and ϕ^0 the initial porosity. The

fluid behavior is described by

$$\frac{d\rho_l}{\rho_l} = \frac{dp}{K_w} \quad (5)$$

where K_w is the fluid bulk modulus. Fluid diffusion is expressed as

$$\frac{\underline{M}}{\rho_l} = \lambda(-\underline{\nabla}(p) + \rho_l \underline{g}) \quad (6)$$

where $\lambda = K_{int}/\mu$ is the fluid diffusivity, K_{int} the intrinsic permeability, and μ the dynamic viscosity. Last, a linear elastic behaviour is assumed for the rock skeleton

$$\underline{\underline{\sigma}}' = \underline{\underline{C}} \underline{\underline{\varepsilon}} \quad (7)$$

where $\underline{\underline{C}}$ is the elasticity tensor that depends on Young's modulus E and Poisson's ratio ν . The parameter values are chosen to be representative of a common situation. Let us assume that for all materials $\nu = 0.25$, and the homogeneous initial material density $\rho_h^0 = 2300 \text{ kg / m}^3$. Table 1 shows the other material properties. In the numerical simulations, the involved fluids are described by water properties, namely, $\rho_l^0 = 1000 \text{ kg / m}^3$, $\mu = 4.33 \times 10^{-4} \text{ Pa.s}$ and $K_w = 2 \text{ GPa}$. Horizontal displacements are set to zero on the lateral boundaries, vertical displacements and fluid flow being set to zero on the lower boundary. Fluid flow is set to zero on the lateral boundaries except along the injection tubing where the loading is applied. On the upper boundary, the vertical total stress and the fluid pressure are set to zero, the reference fluid pressure being equal to the atmospheric pressure. In the present case, the injection process does not influence the pore pressure level and effective stresses on the lateral boundaries (see Figure 2). A confinement coefficient k_i is used to account for the initial stress field. It is defined as the ratio between the horizontal and vertical initial total stress. The vertical initial stress is calculated as the weight of the overlying soil / rock column at each point. The horizontal initial stress only depends on the confinement coefficient. In the following, an extensional stress regime is thus represented by a low confinement coefficient. A compressional stress regime corresponds to a high confinement coefficient. It is worth remembering that an axisymmetric model cannot account for initial stress anisotropy in the horizontal plane. The analysis of failure mechanisms in a strike-slip stress regime (*i.e.*, $\sigma_H > \sigma_v > \sigma_h$) needs a large-scale 3D model.

Effective stress modification due to CO₂ injection

Figure 2 shows how CO₂ injection modifies the effective stress state around the injection zone.

The different load levels are characterized by a normalized injection rate $r = r_e/r_0$, where r_0 is an equivalent injection rate. The equivalent injection rate r_0 corresponds to the level that induces a vertical effective stress equal to zero at the interface between caprock and reservoir. The influence of the loading on the effective stress field at the depth of the injection well is due to a pore pressure rise. The injection influence radius depends on material (hydraulic) properties. The injection influence radius is important in the reservoir because of its high permeability. The effective stress modification observed at the ground level is not generated by a pore pressure rise but by a total stress redistribution. The equilibrium equation (1) is based upon the total stress. The results obtained for the stress state near the ground level should not be taken literally. First, the final stress level depends on the initial stress conditions. The initial horizontal stress state at the ground level is assumed to be zero; this is a reasonable assumption to study deep phenomena but not necessarily surface phenomena. It leads to an overestimation of the stress state at ground level where CO₂ injection takes place. Second, the intensity of the stress state modification on the surface strongly depends on the mechanical properties of the geological layers that are located between the studied geological formation and the surface. In this study, only one upper layer is considered for the sake of simplicity. A more detailed description of the intermediate layers is needed to conclude about stress states close to the ground level.

The stress state modification is particularly important around the injection well. At the injection well depth, the influence of CO₂ injection on the stress state weakens as the distance from the injection tubing increases. Let us focus on the part of the underground that is significantly influenced by the injection. This region of interest is defined in Figure 1. In the

following, the stress changes in that region are extracted from the large-scale calculations. In order to provide a simplified analysis of the consequences of the stress state modification in the region of interest, some assumptions are made on the effective stress field. First, the effective stress field is assumed to depend only on the depth. According to the results of the numerical calculations, this simplifying hypothesis is reasonable everywhere in the region of interest except at a distance of less than 10-20 m around the injection tubing. A specific near-well model is required to study the stress field and its change during the injection process in that zone. However, this has not been carried out in the present study. Second, it is assumed that the effective stress is identical in every direction of the horizontal plane and that the principal stresses are vertical and horizontal. The pressure change and the corresponding stress field that is assumed to be representative of the effective stress field in the region of interest are shown in Figure 3. Injection may lead to important modifications of the horizontal, vertical and shear stresses in the region of interest. The stress state is particularly modified at the interface between caprock and reservoir. For a given injection rate, the pore pressure increase is more uniform in the reservoir than in the caprock or layer 1 because of the high permeability of the reservoir (Figure 3a). A more uniform effective stress state is thus generated in the reservoir compared with the other layers depicted in Figure 3. For the chosen material parameters, various fracture mechanisms may occur depending on initial conditions and injection rate level. Three failure mechanisms are considered, namely, one shear failure mechanism and two tensile failure mechanisms. To study which type of degradation mechanism is activated at the interface between caprock and reservoir, a criterion is associated with each possible fracture regime:

(A) Shear stress induced degradation. Let us consider that a fracture exists at any point with an arbitrary orientation. The shear failure (or shear slip along an existing fracture) risk is calculated with Coulomb's criterion

$$S_{mc} + \sigma_{mc} \sin(\theta) - C_0 \cos(\theta) \geq 0 \quad (8)$$

where $S_{mc} = \frac{1}{2} |\sigma'_h - \sigma'_v|$ denotes the maximum shear stress in the plane σ'_1, σ'_3 and

$\sigma_{mc} = \frac{1}{2} (\sigma'_h + \sigma'_v)$ the mean stress in the plane σ'_1, σ'_3 , where σ'_h is the horizontal effective

stress, σ'_v the vertical effective stress, θ the friction angle (here set to 30°) and C_0 the cohesion

(here set to zero). The behaviour of the large faults is not addressed by the present work.

Concerning the fractures, the impact of their presence on the local stress field is neglected in a

large scale simulation. The post-peak behaviour of the fractures is not studied as the onset of the

propagation / shear slip is considered as the damage measure in a risk analysis approach. A

sensitivity analysis based on a large-scale coupled hydromechanical analysis demonstrated the

prevalent impact of the initial stress ratio on the hydromechanical response of the storage

complex (Rohmer and Seyedi 2009). In the following, the effect of this ratio on the failure

mechanisms is analysed. A pore pressure rise increases the horizontal and vertical effective

stresses σ'_h and σ'_v . This rise does not necessarily lead to an increase of S_{mc} since it depends on

the confinement coefficient and Poisson's ratio. However, a pore pressure rise generates an

increase of σ_{mc} , and this explains why Coulomb's criterion may be activated in various

situations.

(B) Vertical tensile cracking. Rankine's criterion associated with the effective stress in the horizontal direction

$$\sigma'_h \geq 0. \quad (9)$$

(C) Horizontal tensile cracking. Rankine's criterion associated with the effective stress in the vertical direction

$$\sigma'_v \geq 0. \quad (10)$$

Criteria (B) and (C) can be activated by a pore pressure rise.

In situations with low initial horizontal stresses (*i.e.*, $k_i \leq 0.8$), the three mechanisms may be activated as shown in Figure 4, while for moderate and highly confined grounds (*i.e.*, $k_i > 0.8$) only two degradation mechanisms are activated. A loading indicator is introduced to characterize the loading level associated with the activation of criterion (A)

$$C_{mc} = \frac{S_{mc} + \sigma_{mc} \sin(\theta)}{\cos(\theta)} \quad (11)$$

Let us note that if $C_0 \geq C_{mc}$, criterion (A) will not be activated. In Figure 4, when only criterion (A) is activated, the value of C_{mc} is given in MPa by a color map. For a wide range of ground confinements, as the injection rate increases, the first failure mechanism to be activated is due to shear. However, it is difficult to say if it is threatening the storage reliability because the activation of Coulomb's criterion with zero cohesion means that existing cracks may slide, but do not necessarily grow. Furthermore, in the present case, it appears that if the considered shear stress induced mechanism is associated with a cohesion of 5 MPa or more, no shear failure will occur before the activation of an opening failure mode. The importance of this type of mechanism strongly depends on the material behavior and the presence (and orientation) of natural fractures. The loading corresponding to the activation of criterion (C) does not depend on the initial conditions. It also appears that for a confinement coefficient $k_i = 0.8$, the fracture risk is lower because the injection rate leading to the first material degradation is particularly high. The value of $k_i = 0.8$ depends on Poisson's ratio and the geometry of the site.

It was already shown that the likelihood of mechanical failure depends on the anisotropy of initial stress (Rutqvist *et al.* 2008). The present results show that gas injection may provide stress anisotropy too. Shear failure can thus occur for a hydrostatic initial stress state. The orientation of induced shear cracks was not examined in the present study since the most critically oriented existing cracks are considered in each case, which is commonly used as a

conservative approach. However, the results obtained herein illustrate the likelihood of activation of vertical cracks in an extensional stress regime and horizontal cracks in a compressional stress regime. The use of an axisymmetric model provides a better representation of the injection through a vertical well regarding the previous studies based on 2D models especially when the reservoir is equidimensional in a plane view and the horizontal stress state is close to being equibiaxial.

The growth of vertical cracks in opening mode is more problematic for the storage reliability because it generates flow paths towards the surface or the upper layers. This type of cracks is the most likely in cases with relatively low horizontal stresses. A probabilistic cracking model is applied to the case of a low confined ground, i.e. $k_i = 0.7$. The study considers the mode I growth of vertical cracks. Crack growth is assumed as instantaneous compared with the loading rate.

Probabilistic model of crack network growth

Single crack growth

Let us assume that a vertical crack exists in the region of interest shown in Figure 1. Under tensile stresses, it may propagate and leads the failure of caprock. A stress intensity factor criterion based on the effective stress is used to describe the single crack propagation condition

$$K_{Ic} \leq K \quad (12)$$

where K is the stress intensity factor, and K_{Ic} the fracture toughness assumed to be equal to $1 \text{ MPa}\cdot\text{m}^{1/2}$. The present case is approximated by that of a crack propagating in an infinite plane under a polynomial distribution of normal stress varying along the crack direction (Isida, 1976). Simulations of crack propagation were performed over a wide range of initial crack size and depth (Guy *et al.* 2008) and it is shown that if the pressure build-up is high enough in the reservoir to initiate vertical crack, they propagate beyond the horizontal tensile zone. The caprock

may fail before being totally under tensile stresses. In such a case, caprock failure is generated by cracks that are initially located in the reservoir. Both initial size and position have a strong influence on crack initiation (*i.e.*, growth inception). However, the initial size and depth have almost no influence on the tip positions once the crack is fully developed (Guy *et al.* 2008). The active crack tip position mainly depends on the stress distribution and level; it defines the active crack growth. The crack length is approximated as

$$a_c = \alpha_{ac} c^{\beta_{ac}} \quad (13)$$

where $\alpha_{ac} = 100$ m and $\beta_{ac} = 0.5$ are the constants, and c a normalized loading parameter describing the injection

$$c = \frac{r - r_{ini}}{r_{fail} - r_{ini}} \quad (14)$$

with $r_{ini} = 0.75$ the normalized injection rate corresponding to a tensile effective stress appearing at the interface between reservoir and caprock, and $r_{fail} = 1.6$ the normalized injection rate corresponding to caprock failure.

Probabilistic model for crack initiations and interactions

A probabilistic model that takes into account the rock heterogeneity is introduced to describe crack initiation in the caprock under gas injection conditions (Seyedi and Hild 2007). The rock mass heterogeneity corresponds to the presence of defects, *i.e.*, potential cracking sites, with a random distribution. A Poisson point distribution of the micro-fractures is used to model the random character of local failures. An effective density of initial defects is considered to taking into account the effect of the heterogeneity of the stress field in the studied zone (Davies 1973, Hild *et al.* 1992)

$$\lambda_{ft}(c) = \alpha_{Hc} c^{\beta_{Hc}} \lambda_0 \left(\frac{\alpha_{\sigma} c}{\sigma_0} \right)^m \quad (15)$$

where $m = 8$ is the Weibull modulus characterizing the rock heterogeneity, $\sigma_0^m/\lambda_0 = 10^{50}\text{Pa}^m/\text{m}^3$ a scale parameter (Hild and Marquis 1992), $\alpha_{Hc} = 0.22$ and $\beta_{Hc} = 0.25$ are the constants characterizing the stress field heterogeneity, and $\alpha_{\sigma} = \sigma'_h/c$ on the reservoir / caprock interface.

The existence of each initiated crack modifies the stress field in its vicinity. Shielding and amplification zones are created around the crack. A shielding probability is introduced and represents the probability for each crack or potential initiation sites of being located in the shielding zone of a propagating crack. If a potential initiation site is in a shielding zone, it cannot initiate a crack. If a propagating crack lies in a shielding zone its growth is influenced (*i.e.*, stopped) by stress relaxation. For the considered region, the obscuration probability and the initiated crack density read

$$P_{obs}(c) = 1 - \exp\left[-\left(\frac{c}{c_c}\right)^{m+\beta_{Hc}+\beta_{ac}}\right] \quad (16)$$

and

$$\frac{\lambda_b}{\lambda_c}(c) = \left(\frac{m + \beta_{Hc}}{m + \beta_{Hc} + \beta_{ac}}\right) \gamma\left[\frac{m + \beta_{Hc}}{m + \beta_{Hc} + \beta_{ac}}, \left(\frac{c}{c_c}\right)^{m+\beta_{Hc}+\beta_{ac}}\right] \quad (17)$$

where λ_b is the crack density in the region of interest that has a size $Z = l^3$ with $l = 250$ m, γ the incomplete gamma function, λ_c and c_c are the characteristic crack density and characteristic normalized loading variable

$$\lambda_c = \frac{1}{2l\alpha_{ac}} \left[\frac{2l^2\lambda_0\alpha_{ac}\alpha_{Hc}\alpha_{\sigma}^m}{\sigma_0^m} \right]^{\frac{\beta_{ac}}{m+\beta_{Hc}+\beta_{ac}}}, \quad c_c = \left[\frac{\sigma_0^m}{2l^2\lambda_0\alpha_{ac}\alpha_{Hc}\alpha_{\sigma}^m} \right]^{\frac{1}{m+\beta_{Hc}+\beta_{ac}}} \quad (18)$$

As shown in Figure 5, when the load level increases, cracks may initiate and propagate, generating growing stress relaxation zones. The obscuration probability P_{obs} eventually tends to one. When the obscuration probability is close to one, *i.e.* the initiation probability is low, no new crack initiates. This situation is described as the crack network saturation. In the present case, the

crack network saturates quickly after horizontal effective tensile stress appear. At saturation, the number of cracks growing in the region of interest is equal to ten. After network saturation, no additional active crack is initiated and the ten initiated cracks continue to grow and finally lead to caprock failure for a normalized injection rate of 1.6.

Conclusion

This work deals with mechanical changes induced during a CO₂ geological storage operation. The analyses presented herein are based on a simplified, yet realistic, model. The results show that if the gas injection provides important pressure build-up in the reservoir, caprock cracking is likely to occur. The pore pressure rise induced by CO₂ injection around the reservoir may lead to the activation of various cracking mechanisms. To evaluate possible fracturing mechanisms, three criteria based on the effective stress level are introduced, namely Coulomb's criterion, and two Rankine's criteria. The important role of the initial stress regime on the failure of the caprock is illustrated. The type of activated mechanism depends on the initial level of tectonic stresses. For low confined grounds ($k_i \leq 0.8$), as the injection rate increases, the first (Coulomb's) criterion to be satisfied corresponds to a shear induced damage mechanism. The second regime corresponds to the inception of vertical cracks, and the third one to the formation of horizontal cracks. For moderate and highly confined grounds ($k_i \geq 0.8$), the (Rankine's) criterion associated with vertical cracks is likely not to be activated. The results are summarized in a map relating the sustainable injection rate to the initial stress regime. This type of map can be produced for different parameters characterizing the storage sites, and then be used as a fast tool for evaluating sustainable injection scenarios.

The case of a low confined underground leading to vertical crack growth in opening mode is then studied. A probabilistic model is introduced to determine the material cracking state. The

proposed model accounts for the role of rock heterogeneity on its strength and to evaluate the development of crack networks. An injection rate increase after the first crack activation may quickly lead to crack network saturation. Furthermore, the proposed model can be used to directly relate both damage and permeability with the crack length and density. A similar approach may also be used to study the mode II cracking of the material, the first likely cracking fracture mechanism.

Acknowledgments

The present work was funded by the Carnot BRGM Institute. The authors wish to thank Jérémy Rohmer (BRGM/RNSC) for performing diphasic simulation used in the appendix A, and the two anonymous reviewers for their helpful suggestions.

Appendix A: CO₂ equivalent injection rate calculation

A CO₂ equivalent injection rate is introduced in the present work. In this appendix, the pressure build-up in the reservoir calculated by a monophasic (*i.e.*, saturated fluid) model is compared with that calculated through a diphasic simulation considering CO₂ in its supercritical state. To this end, a single layer reservoir capped by two impermeable layers that has a diameter of 100 km and a height of 50 m is considered. Lateral displacement and flow (U_x , M_x) are set to zero on the external boundary. Vertical displacement and flow (U_y , M_y) are set to zero on the upper and lower boundaries of the reservoir layer. The injection is modeled as a prescribed flow on the left border (*i.e.*, symmetry axis). For the diphasic model 0.160 Mt/year of supercritical CO₂ is injected. A monophasic calculation is performed considering the injection of 0.205 Mt/year of water that has the same volume of 0.160 Mt/year of CO₂ with a density of 780 kg/m³.

The initial reservoir pressure is set to $P_0 = 13.7$ MPa corresponding to the medium depth of the reservoir (*i.e.* 1400 m) and an initial saturation liquid density of 1000 kg/m³. For the diphasic

calculation, the initial temperature is set to 42 °C, the Van Genuchten's parameter $\lambda = 0.6$, residual liquid and gas saturation are equal to 20 % and 5 %, respectively, and the air entry pressure is set to 0.05 MPa. The intrinsic permeability of the reservoir is equal to 10^{-14} m^2 . Diphasic simulation is performed using ECO2N module (Pruess 2005) of the code TOUGH2 (Pruess *et al.* 1999). Relative permeability of fluids is modelled through a Van Genuchten-Mualem model (Van Genuchten 1980, Mualem 1976). Hydromechanical couplings are not included in the simulations.

Figure A-1 shows the pressure build-up in the reservoir ($P_{30} - P_0$) after 30 years of injection calculated by both methods. Three different zones are distinguished, namely, the near well zone, the intermediate zone, and the far field zone. Far from the injection well ($r_p \geq 1000 \text{ m}$) the two simulations give almost the same results. At that distance, the reservoir remains saturated even for diphasic calculation and the use of an equivalent injection rate allows us to calculate correctly the pressure field. In the near well zone ($r_p \leq 10 \text{ m}$), the pressure calculated by the monophasic model is very different from that calculated by the diphasic model. The monophasic model yields greater values for the reservoir pressure and this difference amplifies for points nearer to the well. The small viscosity of CO_2 decreases the induced pressure gradient calculated in this zone by the diphasic model. This results show that a monophasic simulation cannot provide good results in terms of pressure build-up in the neighbourhood of the injection well. In the intermediate zone ($10 \text{ m} \geq r_p \geq 1000 \text{ m}$) the overpressure calculated by both models are of the same order of magnitude. The results show that an equivalent injection rate provides an acceptable estimation of the pressure field in this zone. The calculations presented in this work are performed in the region of interest, which is located in the intermediate zone. Consequently, the monophasic equivalence is a good first order approximation.

References

- Bachu, S., 2003. Screening and ranking of sedimentary basins for sequestration of CO₂ in geological media. *Environmental Geology*, **44**, 277-289.
- Biot, M. A., 1941. General theory of three dimensional consolidation. *Journal of Applied Physics*, **12**, 155-164.
- Davies D.G.S., 1973. The Statistical Approach to Engineering Design in Ceramics. *Proc. Brit. Ceram. Soc.*, **22**, 429-452.
- EDF R&D. 2008. Code_Aster, Code d'Analyses des Structures et Thermomécanique pour Etudes et Recherches, <http://www.code-aster.org>.
- Guy N., Seyedi M., Hild F., 2008. Hydro-mechanical modeling of underground CO₂ storage and risk evaluation through a probabilistic fracturing model, 12th IACMAG, CO8.pdf, 8 p., Goa (India), October 1-6.
- Hild F., Billardon R., Marquis D., 1992. Hétérogénéité des contraintes et rupture des matériaux fragiles. *C. R. Acad. Sci. Paris*, t. 315, Série II, 1293-1298.
- IPCC, 2005. IPCC special report on carbon dioxide capture and storage. Prepared by working group III of the Intergovernmental Panel on Climate Change [Metz B, Davidson O, de Coninck HC, Loos M, Meyer LA (Edts.)]. Cambridge University Press, Cambridge, United Kingdom/ New York, USA.
- Isida M. 1976. Elastic analysis of cracks and stress intensity factors, *Fracture mechanics and strength of materials 2*, Baifuukan, p. 128.
- Mualem, Y. 1976. A new model for predicting the hydraulic conductivity of unsaturated porous media. *Water resources*, **12**, 513-521.
- Pruess, K., Oldenburg C.M. and Moridis G.J. 1999. TOUGH2 user's guide, version 2.0. Technical report LBNL-43134, Lawrence Berkley National Laboratory.
- Pruess, K. 2005. ECO2N – a TOUGH2 fluid property module for mixture of water, NaCl and CO₂. Technical report LBNL-57952, Lawrence Berkley National Laboratory.
- Rohmer, J. and Seyedi, D.M., In press. Coupled large scale hydromechanical modelling for caprock failure risk assessment of CO₂ storage in deep saline aquifers. *Oil & Gas Science and Technology – Rev. IFP*, doi:10.2516/ogst/2009049.
- Rozhko, A.Y., Podladchikov, Y.Y. and Renard, F., 2007. Failure patterns caused by localized rise in pore-fluid overpressure and effective strength of rocks. *Geophysical Research Letters*, **34**, L22304, doi:10.1029/2007GL031696.
- Rutqvist, J., Birkholzer, J.T. and Tsang, C.F., 2008. Coupled reservoir geomechanical analysis of the potential for tensile and shear failure associated with CO₂ injection in multilayered reservoir caprock systems. *Int J Rock Mechanics & Mining Science*, **45**, 132-143.
- Seyedi M., Hild F., 2007. Towards a probabilistic model for the formation of crack networks in rocks, *Revue Française de Géotechnique*, **119**, 73-82
- Soltanzadeh, H. and Hawkes, C.D., 2009. Assessing fault reactivation tendency within and surrounding porous reservoirs during fluid production or injection. *Int J Rock Mechanics & Mining Sciences*, **46**, 1-7.
- Van Genuchten. 1980. A closed-form equation for predicting the hydraulic conductivity of unsaturated soils. *Soil Science Society of America Journal*, **44**, 892-898.
- Vidal-Gilbert, S., Nauroy, J.-F., Brosse E., 2009. 3D geomechanical modelling for CO₂ geologic storage in the Dogger carbonates of the Paris Basin. *Int. J. of Greenhouse Gas Control*, **3**, 288-299.

Table 1. Material properties

Material	E (GPa)	K_{int} (m ²)	ϕ^0	b
Soil	1	10^{-12}	0.3	1.0
Layer 0	20	10^{-15}	0.15	0.8
Cap rock	20	10^{-17}	0.05	0.8
Host rock	20	10^{-14}	0.15	0.8
Layer 1	20	10^{-17}	0.05	0.8
Layer 2	20	10^{-15}	0.15	0.8

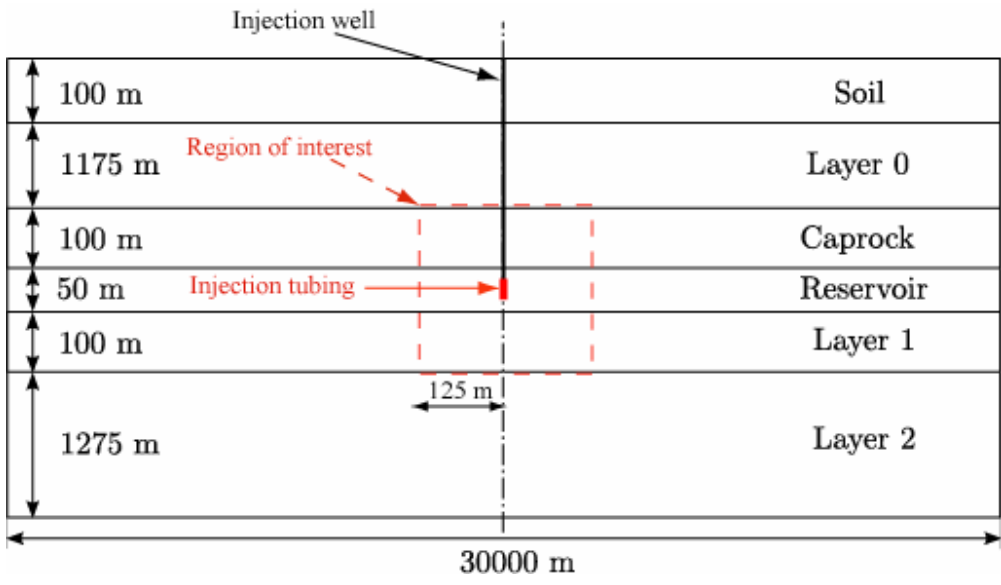


Figure 1. Model geometry and definition of the region of interest.

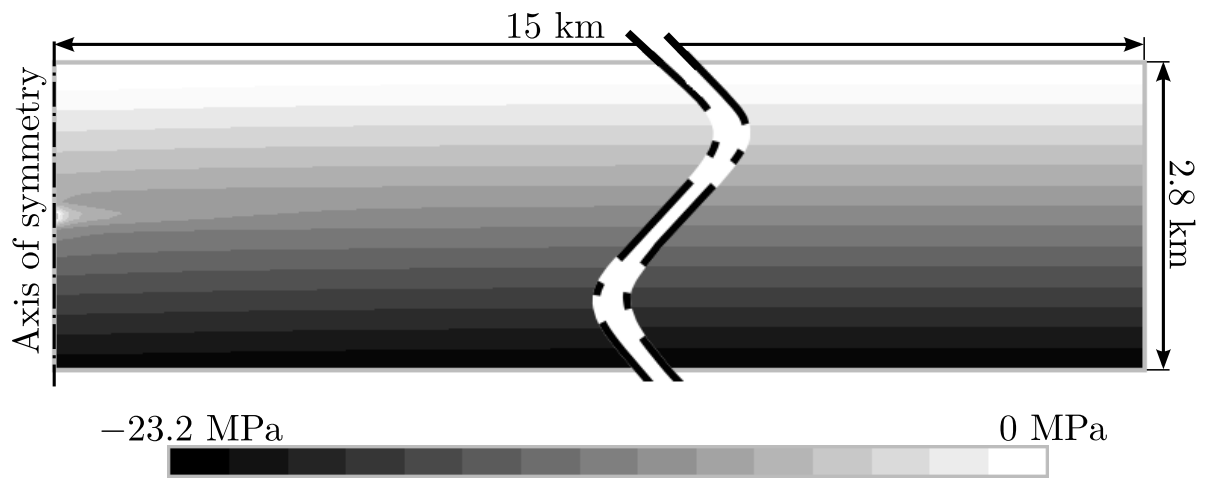


Figure 2. Horizontal effective stress in the underground for a normalized injection rate $r = 1$ with a confinement coefficient $k_i = 0.7$.

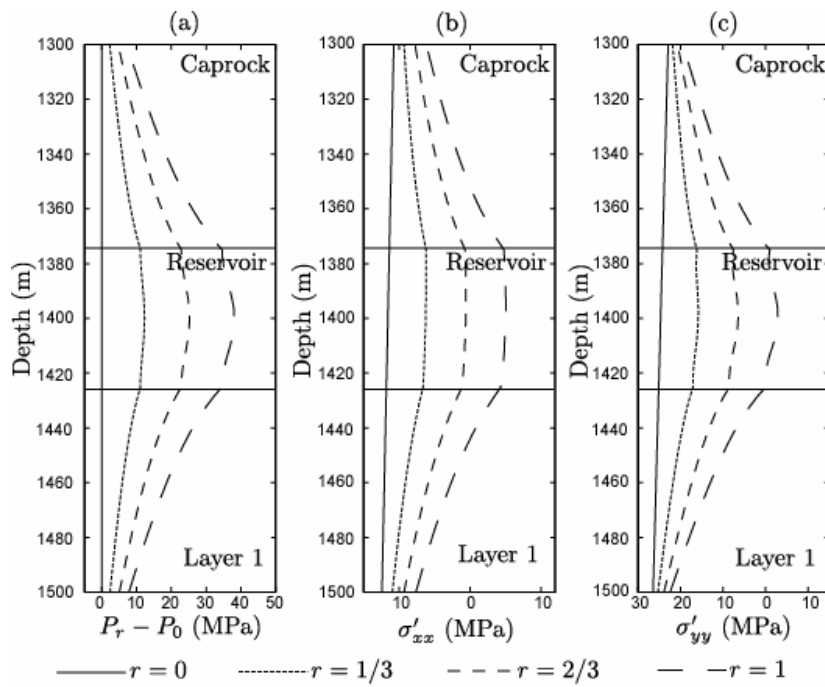


Figure 3. Pressure change (a), horizontal (b) and vertical (c) effective stress along the studied line for $k_i = 0.7$ and several equivalent injection rates.

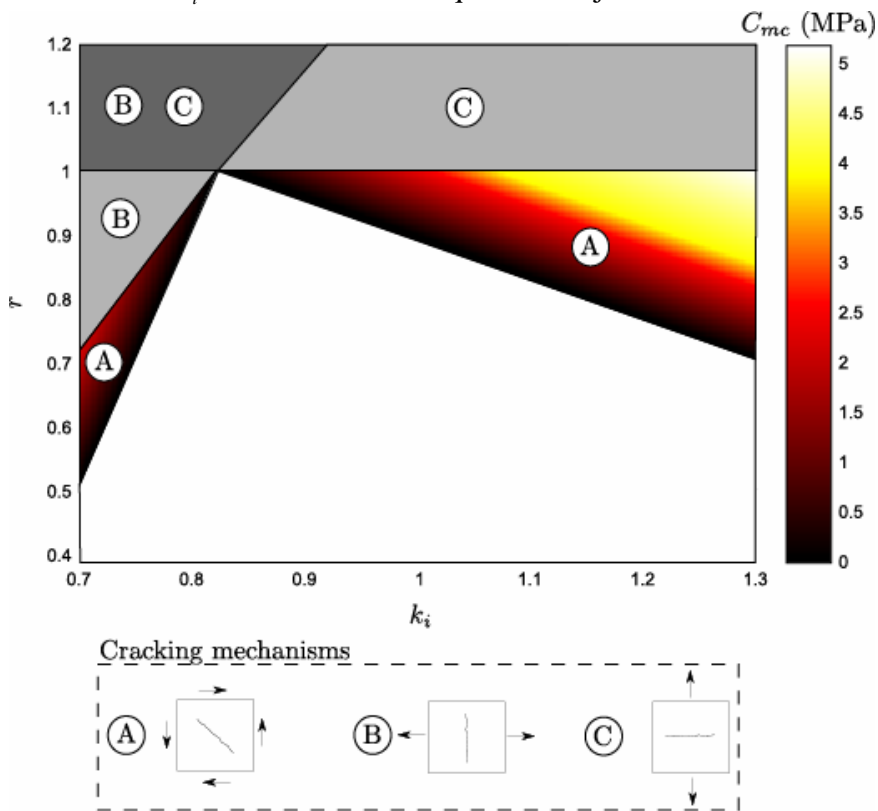


Figure 4. Map of cracking mechanisms for different confinement and injection rates.

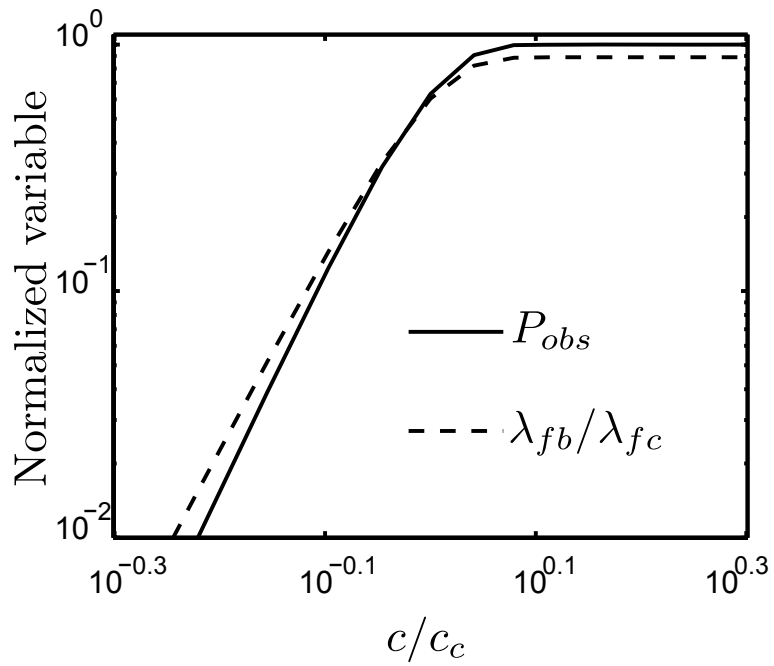


Figure 5. Obscuration probability and normalized crack density as a function of normalized loading parameter

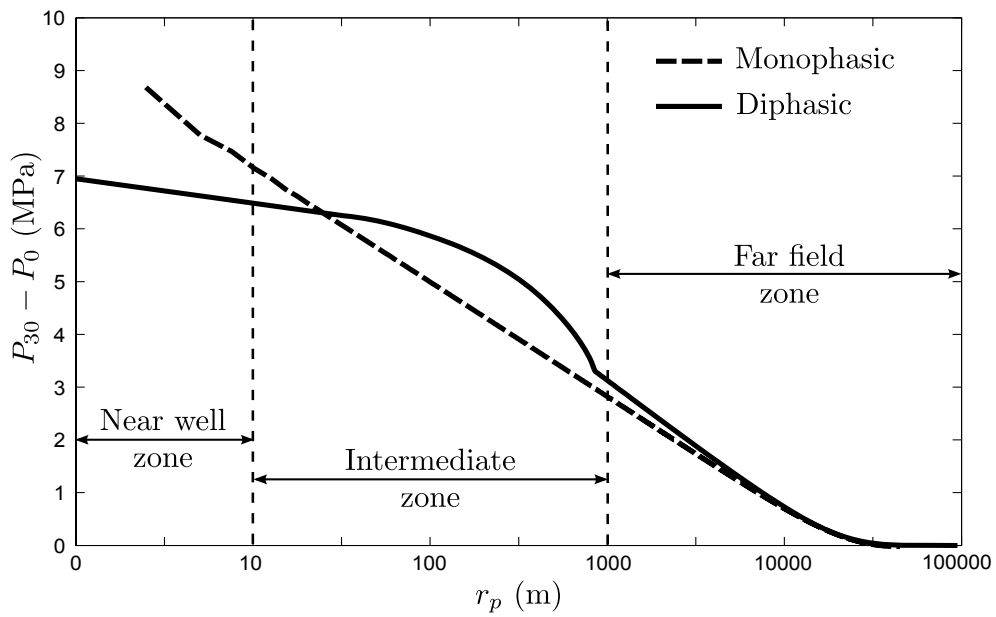


Figure A-1. Pressure field in the reservoir as a function of distance from the injection well after 30 years of injection.